Available online at www.sciencedirect.com
SCIENCE DIRECT®
International Journal of Heat and Mass Transfer 47 (2004) 1783–1798
International Journal of HEAT and MASS TRANSFER
www.elsevier.com/locate/ijhmt

Thermal conductivity decomposition and analysis using molecular dynamics simulations. Part I. Lennard-Jones argon

A.J.H. McGaughey, M. Kaviany *

Department of Mechanical Engineering, University of Michigan, 2250 G.G. Brown Laboratory, 2350 Hayward Avenue, Ann Arbor, MI 48109-2125, USA

Received 10 February 2003; received in revised form 13 October 2003

Abstract

Using molecular dynamics simulations and the Green–Kubo method, the thermal transport in the Lennard-Jones argon face centered cubic crystal is described by two time constants related to the decay of the heat current autocorrelation function. The first time scale is associated with short wavelength acoustic phonons that have mean free paths equal to one half of their wavelength. The associated thermal conductivity is independent of temperature, and has a value around 0.09 W/m K. The second time scale is longer, and corresponds to acoustic phonons with mean free paths longer than one half of their wavelength. The associated thermal conductivity is temperature dependent, and ranges from 3.92 W/m K at a temperature of 10 K to 0.08 W/m K at a temperature of 100 K. This decomposition allows for a comparison of the crystal phase results with those from corresponding amorphous and liquid phases.

1. Introduction

Heat transfer in a dielectric solid, where the electrons are tightly bound to the atomic nuclei, is realized through the transport of phonons, quanta of energy associated with lattice vibrations. To predict the thermal conductivity of such materials, existing analysis techniques require numerous simplifications and assumptions before solvable forms are obtained, and are unable to take into account structural details at the atomic level. There is limited application of these methods to new and complex materials. Furthermore, these approaches deal with analysis in phonon space, and can be difficult to relate to the physical structure of the material.

In applications of the Boltzmann transport equation (BTE) under the relaxation time approximation to predict the thermal conductivity, it is commonly assumed that only acoustic phonons contribute to the thermal transport, and a simplified form of the phonon dispersion relation is often used. Furthermore, the temperature and frequency dependencies of the relaxation times must be specified, and the results must be fitted to the experimental data. In some cases, a single relaxation time is assumed to be valid for all phonon modes. This approach has been used to analytically and numerically investigate silicon [1–3], germanium [1,4,5] and alumina [6].

In the application of the gas kinetic theory formulation to the solid state, the thermal conductivity, k, is given by [7]

$$k = \frac{1}{3}\rho \sum_i c_{v,i} u_i \Lambda_i = \frac{1}{3}\rho \sum_i c_{v,i} u_i^2 \tau_{\mathrm{K},i}, \tag{1}$$

where the summation is over the $3N$ phonon (normal) modes of the system (where N is the total number of atoms), ρ is density, and $c_{v,i}$, u_i, Λ_i and $\tau_{\mathrm{K},i}$ are the mode dependent specific heat, phonon speed, phonon mean free path, and kinetic theory phonon relaxation time, respectively.

The specification of all the parameters in Eq. (1) for even a nanometer sized system is a formidable task, as many of them are not readily predicted or available.

* Corresponding author. Tel.: +1-734-936-0402; fax: +1-734-647-3170.
E-mail address: kaviany@umich.edu (M. Kaviany).

0017-9310/$ - see front matter © 2003 Elsevier Ltd. All rights reserved.
doi:10.1016/j.ijheatmasstransfer.2003.11.002

Nomenclature

a	lattice constant, constant
A	constant
b	constant
B	constant
c_v	specific heat at constant volume
E	energy (kinetic and potential)
f	frequency
$\mathbf{F}$	force
$\hbar$	Planck constant/2π, 1.0546×10^{-34} J s
k_B	Boltzmann constant, 1.3806×10^{-23} J/K
k	thermal conductivity
l_{td}	length scale in transient diffusion time
m	Lennard-Jones mass scale, 6.63×10^{-26} kg
n	number density of atoms (N/V)
N	number of atoms
p	pressure
$\mathbf{q}$	heat current vector
$r, \mathbf{r}$	particle position, interparticle separation
t	time
T	temperature
u	phonon speed
U	potential energy
$\mathbf{v}$	particle velocity
V	volume
x	$\hbar\omega/k_BT$

Greek symbols

α	thermal diffusivity
β	deviation of MD specific heat from classical-harmonic value
ϵ	Lennard-Jones energy scale, 1.67×10^{-21} J
κ	wave number
Λ	phonon mean free path
ρ	density
σ	Lennard-Jones length scale, 3.40×10^{-10} m
τ	time constant
ω	angular frequency

Subscripts

ac	acoustic
CP	Cahill–Pohl
D	Debye
equ	equilibrium
i	summation index, particle label, intermediate
j	summation index, particle label
lg	long range
nn	nearest neighbor
o	self (referring to a particle)
K	kinetic
LJ	Lennard-Jones
sh	short range
td	transient diffusion
V	Volz et al. model

Hofmeister [8] has used such an approach with appropriate simplifications and fitting parameters to predict the thermal conductivity of materials in the earth's mantel.

Integration of Eq. (1) over all phonon modes leads to

$$k = \frac{1}{3}\rho c_v u \Lambda = \frac{1}{3}\rho c_v u^2 \tau_K, \tag{2}$$

where c_v, u, Λ and τ_K are now average values. The specific heat is the bulk value, and the phonon speed is generally taken as some mean speed of sound in the material. The value of the mean free path/relaxation time is fitted from experimental results for the other parameters. Thus, Eq. (2) cannot be used to predict the thermal conductivity.

Cahill and Pohl (CP) [9,10] have proposed a model for the thermal conductivity of amorphous solids, given by

$$k_{CP} = \left(\frac{\pi}{6}\right)^{1/3} k_B n^{2/3} \sum_i \left[u_i \left(\frac{T}{T_i}\right)^2 \int_0^{T_i/T} \frac{x^3 e^x}{(e^x-1)^2} dx \right], \tag{3}$$

where T_i is defined as $u_i(\hbar/k_B)(6\pi^2 n)^{1/3}$, x is $\hbar\omega/k_BT$, k_B is the Boltzmann constant, n is the number density of atoms, T is temperature, $\hbar$ is the Planck constant divided by 2π, ω is angular frequency, and the summation is over the three sound modes of the solid (one longitudinal and two transverse). This model is an extension of the Einstein thermal conductivity [10,11]. The mean free path of every phonon is assumed to be equal to one half of its wavelength, the smallest physically meaningful value it can take on. The predictions of a phenomenologically similar model have been interpreted as a minimum thermal conductivity [12]. Experimental measurements of a range of amorphous solids have not yielded any thermal conductivities significantly below k_{CP} [10].

Molecular dynamics (MD) simulations, where the position and momentum space trajectories of a system of particles are predicted using the Newton second law of motion, offer an alternative approach. No assumptions about the nature of the thermal transport are required before predicting the thermal conductivity. The only inputs are an atomic structure and appropriate interatomic potential, which can be constructed from

experimental and/or ab initio results. Observations at the atomic level, not possible in experiments, can be made.

Molecular dynamics has been used to predict the thermal conductivities of a wide variety of dielectric solids and liquids with varying degrees of success [13–29]. Challenges include finding suitable interatomic potentials and taking into account size effects that result from computational limits (e.g., a finite sized simulation cell imposes an upper limit on the allowed phonon wavelengths). Much of the work has focused on the prediction of the bulk phase thermal conductivity, and not on the atomic level features and mechanisms that are responsible for it.

In this series of two papers, a methodology is presented by which the thermal conductivity of a dielectric crystal can be decomposed into distinct components associated with different length and time scales. In conjunction with other data extracted from the simulations, the thermal conductivity can then be related to the atomic structure. In this paper, Part I, the concepts and ideas are formulated and developed through the use of the Lennard-Jones (LJ) argon face centered cubic (fcc) crystal, amorphous, and liquid phases, and then applied to complex silica structures in the following paper [30] (referred to hereafter as Part II).

Here, the techniques available for predicting the thermal conductivity of a dielectric material using MD are reviewed. The MD simulation procedures are described. The thermal conductivity decomposition is introduced, applied to the LJ argon fcc crystal, and validated through comparisons to analytical predictions, MD results for the thermal conductivity of the corresponding amorphous and liquid phases, and particle–particle energy correlation functions. The multiple time constants extracted from the decomposition are shown to have a physical basis not found for the single time constants in the kinetic theory and BTE models. The cumulative frequency dependence of the thermal conductivity predicted by the MD and BTE approaches is also examined.

2. Molecular dynamics thermal conductivity prediction

Three main techniques have been developed to predict the thermal conductivity of a dielectric material using MD simulations. These are the Green–Kubo (GK) approach (an equilibrium method), a direct application of the Fourier law of conduction (a steady state, non-equilibrium method, sometimes called the direct method), and unsteady methods. The majority of recent investigations have used one of the first two methods, and these are discussed here.

The net flow of heat in a solid, given by the heat current vector $\mathbf{q}$, fluctuates about zero at equilibrium. In the GK method, the thermal conductivity is related to how long it takes these fluctuations to dissipate, and for an isotropic material is given by [31]

$$k = \frac{1}{k_B V T^2} \int_0^\infty \frac{\langle \mathbf{q}(t) \cdot \mathbf{q}(0) \rangle}{3} \mathrm{d}t, \tag{4}$$

where V is the volume of the simulation cell, t is time, and $\langle \mathbf{q}(t) \cdot \mathbf{q}(0) \rangle$ is the heat current autocorrelation function (HCACF). In materials where the fluctuations are long lived (i.e., the mean free path of phonons is large), the HCACF decays slowly. The thermal conductivity is related to the integral of the HCACF, and is accordingly large. In materials such as amorphous solids, where the mean free path of phonons is small, thermal fluctuations are quickly damped, leading to a small integral of the HCACF and a low thermal conductivity. The heat current vector is given by [31]

$$\mathbf{q} = \frac{\mathrm{d}}{\mathrm{d}t} \sum_i \mathbf{r}_i E_i, \tag{5}$$

where the summation is over the particles in the system, and $\mathbf{r}$ and E are the position vector and energy (kinetic and potential) of a particle, respectively. For a pair potential, such as the LJ potential, Eq. (5) can be recast as [31]

$$\mathbf{q} = \sum_i E_i \mathbf{v}_i + \frac{1}{2} \sum_{i,j} (\mathbf{F}_{ij} \cdot \mathbf{v}_i) \mathbf{r}_{ij}, \tag{6}$$

where $\mathbf{v}$ is the velocity vector of a particle, and $\mathbf{r}_{ij}$ and $\mathbf{F}_{ij}$ are the interparticle separation vector and force vector between particles i and j, respectively. This form of the heat current is readily implemented in an MD simulation.

The GK method has been used in simulations of LJ argon [15,17,22], β-silicon carbide [18], diamond [21], silicon [24,29], amorphous silicon [14], germanium based materials [25], and nanofluids [28]. The main challenge is the specification of the integral in Eq. (4). This aspect of the GK method will be addressed in detail in Sections 5.1 and 5.2.

In the direct method, a one-dimensional temperature difference is imposed on a simulation cell. The resulting heat flux is used to determine the thermal conductivity using the Fourier law of conduction. As an alternative, a heat flux can be imposed, and the resulting temperature profile determined. To allow long wavelength modes to exist and to minimize the effects of thermal boundary resistances at the hot and cold sinks (i.e., to reduce size effects), the simulation cell is often taken to be long in the direction of the temperature gradient. The application of a temperature difference on the order of 10 K to a nanometer sized sample results in very large heat fluxes, and non-linear temperature profiles can develop. The use of the direct method is questionable in these cases. This method has been used to predict the thermal

conductivity of amorphous silica [19], zirconia and yttria-stabilized zirconia [26], LJ systems [23,27], and various liquids [16,20]. Schelling et al. [29] address the size effects for silicon by predicting the thermal conductivity for a range of simulation cell sizes, and taking a limit of the results as the cell size goes to infinity. Good agreement with GK predictions is found at a temperature of 1000 K.

The GK method is used in the current investigation. As will be seen, it allows for the extraction of information not accessible in the direct method. It is also advantageous for the large unit cell crystals to be discussed in Part II, where large simulation cells would be required to get well defined temperature profiles. The electronic component of the thermal conductivity for all cases considered is assumed negligible. This is a very good assumption for the van der Waals solids (such as argon), which have filled electron shells.

3. Simulation procedures

As a starting point for investigating what MD simulations can reveal about the nature of atomic level thermal transport in dielectrics, materials described by the LJ potential are considered. Choosing a simple system allows for the elucidation of results that may be difficult to resolve in more complex materials, where multi-atom unit cells (and thus, optical phonons) can generate additional effects. The LJ atomic interactions are described by the pair potential [32]

$$U_{ij}(r_{ij}) = 4\epsilon\left[\left(\frac{\sigma}{r_{ij}}\right)^{12} - \left(\frac{\sigma}{r_{ij}}\right)^{6}\right], \tag{7}$$

where U_{ij} is the potential energy associated with particles i and j (i not equal to j). The depth of the potential energy well is ϵ, and corresponds to an equilibrium particle separation of $2^{1/6}\sigma$. The LJ potential describes the noble elements well. Argon, for which σ and ϵ have values of 3.40×10^{-10} m and 1.67×10^{-21} J, respectively [32], is chosen for the current investigation. The fcc crystal, amorphous and liquid phases are considered. The 12 nearest neighbors of an atom in the fcc crystal and amorphous structures are shown in Fig. 1(a) and (b), respectively. In the fcc crystal all atoms are at equivalent positions, and the atomic displacements are isotropic. In the amorphous phase each atom has a unique environment, with a range of neighbor orientations and bond lengths. The resulting atomic displacements are anisotropic.

All reported data correspond to simulations in the *NVE* (constant mass, volume and energy) ensemble at zero pressure with a time step of 4.285 fs. This time step was found to be sufficient to resolve the phenomena of interest (e.g., the smallest time scale of interest in the heat current is about twenty time steps). The simulation cell is cubic and contains 256 atoms. In similar simulations, Kaburaki et al. [17] have found good agreement between the fcc crystal thermal conductivities predicted from cells containing 256 and 500 atoms. This result indicates that 256 atoms are sufficient to eliminate size effects. Periodic boundary conditions are imposed in all directions. The equations of motion are integrated with a Verlet leap-frog algorithm [33]. The atomic interactions are truncated and shifted at a cutoff radius that is one half of the length of the simulation cell (so as to include as many atoms as possible in the dynamics), and the pressure is corrected as given by Frenkel and Smit [34]. For the fcc crystal, temperatures between 10 and

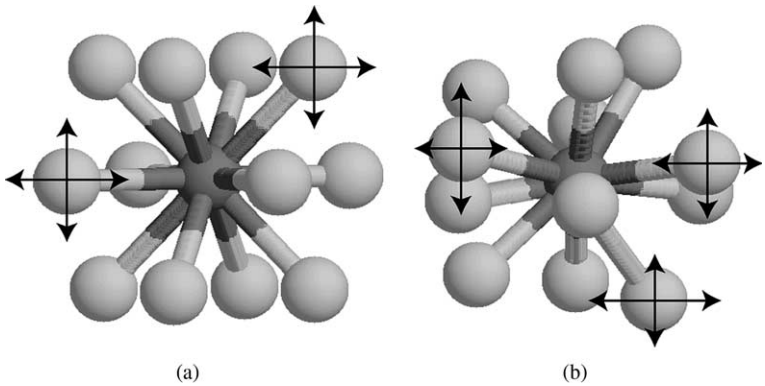

Fig. 1. Local environment for an atom in (a) the fcc crystal and (b) the amorphous structure. In the crystal, there are 12 nearest neighbors. For the amorphous phase, the 12 nearest atoms are shown. While the color of the center atom is a darker gray than the neighbors, all the atoms are the same. Also shown are representative atomic displacements (not to scale) for some of the neighbor atoms for each case. The motions in the fcc crystal are isotropic and equivalent between atoms, while those in the amorphous structure are not.

100 K are considered in 10 K increments. Melting occurs above a temperature of 100 K. The amorphous phase is generated by heating the fcc crystal to a temperature of 300 K, running for 10^4 time steps to eliminate any memory of the initial configuration, and then quenching at 8.5×10^{11} K/s back to a temperature of 10 K. The amorphous phase is stable up to a temperature of 20 K. Above this point, the equilibrium thermal fluctuations in the system are large enough to return the atoms to the fcc crystal structure. This is consistent with previous findings [22]. Temperatures of 10, 15, and 20 K are considered. The liquid phase is obtained by heating the amorphous phase until melting occurs. Using this approach, a stable liquid is found to exist at temperatures as low as 80 K. Due to the small length and time scales used, the melting temperature, which experimentally is 83.8 K, is not well defined, and it is possible to have stable fcc crystal and liquid phases at the same temperature and pressure, although the densities are different. Temperatures of 80, 90, and 100 K are considered for the liquid simulations.

As described, the MD simulations are classical. The use of quantum corrections at low temperatures in MD simulations is still under discussion. While some have found improved agreement with experimental results when the temperature and thermal conductivity are appropriately scaled [18,24], others have shown that the corrections are negligible [21]. There are many other factors that contribute to the success of a simulation in reproducing experimental results (e.g., the suitability of the interatomic potential and the size of the simulation cell). For argon, quantum effects are not expected to be significant [32], and no corrections are made.

To determine the zero pressure cell size (which is temperature dependent), simulations were run in the *NpT* (constant mass, pressure and temperature) ensemble at the temperatures of interest. The temperature and pressure were controlled with a Nose-Hoover thermostat and a Berendsen barostat [35]. After an initialization period of 2×10^5 time steps (0.857 ps), the zero pressure cell size was found by averaging the value of the cell size over a further 2×10^5 time steps. The potential energy of the system as a function of temperature was also determined, and is used in the temperature setting procedure in subsequent simulations.

In all subsequent simulations discussed, an initialization period of 5×10^5 time steps has been used. The system is run in the *NVT* (constant mass, volume and temperature), ensemble for 3×10^5 time steps. To set the temperature for the *NVE* ensemble, the potential energy of the system is then monitored every time step. When it reaches a value within 10^{-4}% of the desired potential energy (this generally takes less than 5000 time steps), the ensemble is switched to *NVE*, and the system is run until the total number of time steps is 5×10^5. While running in the *NVE* ensemble, the total energy is conserved to within 0.005%.

The thermal conductivity is calculated using the GK method as described in Section 2. All simulations used in these calculations consist of an additional 10^6 time steps over which the heat current vector is calculated every five time steps. A correlation length of 5×10^4 time steps with 2×10^5 time origins is used in the autocorrelation function. For all cases, five independent simulations (with random initial velocities) are performed and the HCACFs are averaged before finding the thermal conductivity. This ensures a proper sampling of phase space [18]. For the fcc crystal at a temperature of 10 K, where the correlation time is long, 10 independent simulations are performed. For the energy correlation data, a further 10^5 time steps are run beyond the initialization period, during which the atomic energies are calculated every time step.

4. Prediction of system parameters from Lennard-Jones potential

4.1. Unit cell size

When relaxed to zero temperature, the MD fcc crystal unit cell parameter, a, is 5.2414 Å, which corresponds to a cutoff radius of 3.1σ. The experimental value is 5.3033 Å [32]. Li [22] has found values of 5.3050 Å for a cutoff radius of 2.5σ, and 5.2562 Å for a cutoff radius of 5σ.

The lattice constant can also be predicted from the analytical form of the LJ potential. To do this, the total potential energy associated with one atom, U_i, must be considered. If the energy in each pair interaction is assumed to be equally distributed between the two atoms, U_i will be given by

$$U_i = \frac{1}{2}\sum_{i\neq j} U_{ij}, \tag{8}$$

which for the fcc crystal lattice can be expressed as [32]

$$U_i = 2\epsilon\left[A_{12}\left(\frac{\sigma}{r_{\mathrm{nn}}}\right)^{12} - A_6\left(\frac{\sigma}{r_{\mathrm{nn}}}\right)^{6}\right], \tag{9}$$

where A_{12} and A_6 have values of 12.13 and 14.45, respectively, and r_{nn} is the nearest neighbor separation. By setting

$$\frac{\partial U_i}{\partial r_{\mathrm{nn}}} = 0, \tag{10}$$

the equilibrium value of r_{nn} is found to be

$$r_{\mathrm{nn,equ}} = \left(\frac{2A_{12}}{A_6}\right)^{1/6}\sigma = 1.09\sigma. \tag{11}$$

For argon, the equilibrium separation of Eq. (11) corresponds to a unit cell parameter of 5.2411 Å, which agrees with the zero temperature MD result to within less than 0.01%. This gives confidence to the simulation procedures used. Differences between the current MD results and those of Li [22] can be attributed to the form of the potential cutoff used and the pressure calculation method.

4.2. Period of atomic oscillation and energy transfer

In a simplified, real space model of atomic level behavior, the energy transfer between neighboring atoms can be assumed to occur over one half of the period of oscillation of an atom [10,11]. The associated time constant can be estimated from the Debye temperature, T_D, as

$$\tau_D = \frac{2\pi\hbar}{2k_B T_D}. \tag{12}$$

The factor of two in the denominator is included as one half of the period of oscillation is desired. By fitting the specific heat (as predicted by the MD zero temperature phonon density of states) to the Debye model, the Debye temperature is found to be 89 K. This compares well to the experimental value of 85 K [37]. The MD result is used in subsequent calculations, and gives a τ_D value of 0.270 ps (~63 time steps).

An estimate of this time constant can also be made using the LJ potential. The time constant is related to the curvature of the potential well that an atom experiences at its minimum energy. Assuming that the potential is harmonic at the minimum, the natural frequency of the atom will be given by

$$\omega = \left(\frac{1}{m} \frac{\partial^2 U_i}{\partial r_{nn}^2}\bigg|_{r_{nn}=r_{nn,equ}} \right)^{1/2} = 22.88\left(\frac{\epsilon}{\sigma^2 m}\right)^{1/2}, \tag{13}$$

where m is the mass of one atom, which for argon is 6.63×10^{-26} kg, and U_i and $r_{nn,equ}$ are taken from Eqs. (9) and (11), respectively. One half of the period of oscillation is then

$$\tau_{LJ} = \frac{1}{2}\frac{1}{2\pi\omega} = 0.00348\left(\frac{\sigma^2 m}{\epsilon}\right)^{1/2}, \tag{14}$$

which evaluates to 0.275 ps, within 2% of τ_D.

The physical significance of this time constant can be further investigated by considering the flow of energy between atoms in the MD simulation cell. This is done by constructing energy correlation functions between an atom and its 12 nearest neighbors. The calculations are based on the deviations of the particle energies from their mean values. As all the atoms in the fcc crystal simulation cell are at equivalent positions, the results can be averaged over neighbors, space, and time. The resulting correlations for the fcc crystal are shown in Fig. 2 for all temperatures considered. The curves are normalized against their zero time value to allow for comparison between the different temperatures. Similar calculations have been made for the amorphous phase.

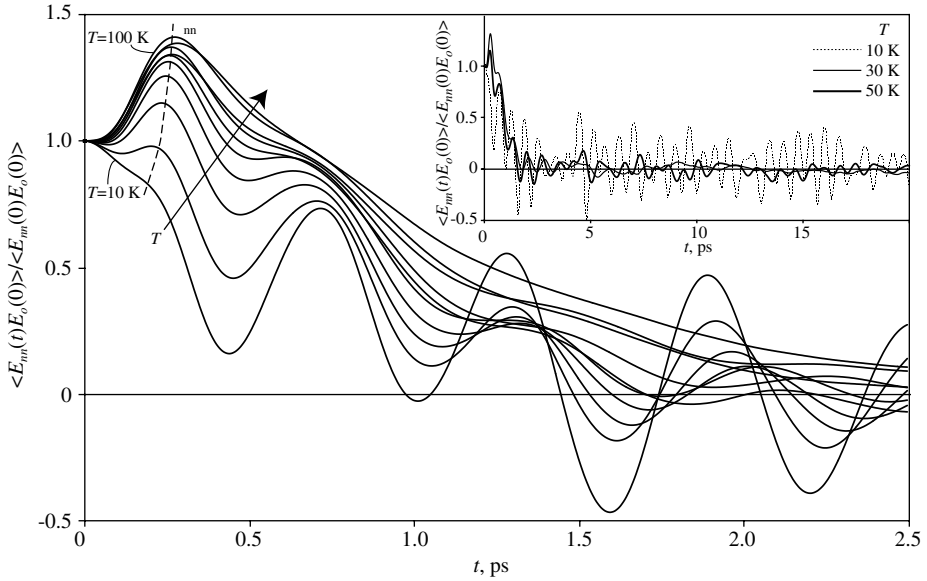

Fig. 2. Nearest neighbor particle–particle energy correlation functions for the fcc crystal. The energy data correspond to deviations from the mean values. A longer time scale is shown for $T = 10$, 30, and 50 K in the inset plot, where the decrease in the long time coherence at higher temperatures is evident.

Table 1
Thermal conductivity decomposition parameters and predicted values. The value of k given for the fcc crystal and liquid phases is from the exponential fits, while that for the amorphous phase is specified directly from the integral of the HCACF

Structure	T, K	ρ, kg/m^3	τ_{nn}, ps	$\tau_{ac,sh}$, ps	$\tau_{ac,lg}$, ps	$k_{ac,sh}$, W/m K	$k_{ac,lg}$, W/m K	k, W/m K
Fcc crystal	10	1820	–	0.285	23.0	0.082	3.92	4.00
	20	1801	0.206	0.264	9.52	0.078	1.49	1.57
	30	1780	0.236	0.269	5.69	0.087	0.816	0.903
	40	1756	0.248	0.264	3.79	0.091	0.483	0.574
	50	1729	0.257	0.268	2.93	0.100	0.316	0.417
	60	1701	0.261	0.266	2.47	0.106	0.225	0.331
	70	1671	0.265	0.252	1.65	0.102	0.141	0.243
	80	1639	0.265	0.246	1.50	0.105	0.112	0.218
	90	1597	0.274	0.222	0.900	0.093	0.079	0.172
	100	1541	0.283	0.187	0.486	0.067	0.077	0.144
Amorphous	10	1727	0.257	–	–	–	–	0.179
	15	1716	0.261	–	–	–	–	0.176
	20	1705	0.261	–	–	–	–	0.180
				τ_1, ps				
Liquid	80	1450	–	0.204	–	–	–	0.137
	90	1392	–	0.207	–	–	–	0.123
	100	1328	–	0.211	–	–	–	0.110

In this case, the number of nearest neighbors used is based on a uniform cutoff that gives an average value of 12 for the entire system, and the spatial averaging is assumed to be valid.

The first peak locations, which we denote as τ_{nn}, for the crystal and amorphous phases are given in Table 1. The resolution in the values is one time step, which is about 0.004 ps. For the crystal, the value of τ_{nn} increases with temperature, which is due to the decreasing density (also given in Table 1). As the atomic separation increases, it takes longer to transfer energy between two atoms. This density dependence is confirmed by the amorphous results. At temperatures of 10 and 20 K, where the densities are very close to the fcc crystal values for temperatures of 50 and 60 K, the values of τ_{nn} are indistinguishable from the fcc crystal values. Between temperatures of 40 and 100 K, the time constants τ_D, τ_{LJ} and τ_{nn} agree to within 10%. This agreement supports the assumed link between the period of atomic oscillation and the time scale of the atom to atom energy transfer. The τ_{nn} results at low temperature will be addressed in Section 5.2.2.

5. Results and analysis

5.1. Heat current autocorrelation function

The HCACF and its integral (whose converged value is related to the thermal conductivity through Eq. (4)) are shown in Fig. 3(a) and (b) for all cases considered. The HCACF is normalized by its zero time value to allow for comparisons between the different temperatures. The integral is calculated using the trapezoidal rule. Longer time scales are shown for the fcc crystal in Fig. 4(a)–(c) for temperatures of 10, 50, and 100 K, respectively. Note that as the temperature increases, the HCACFs of the three phases are approaching each other.

The fcc crystal HCACF shows a two stage behavior. There is an initial drop, similar for all cases, followed by a longer decay, whose extent decreases as the temperature increases. We believe that the oscillations in the secondary decay are a result of the periodic boundary conditions. This hypothesis is supported by results obtained using larger unit cells, where the period of the oscillations increases as the cell size increases (not shown). The integral of the HCACF converges well, and the thermal conductivity can be specified directly from the graph by averaging the integral over a suitable range. To remove the subjective judgment, Li et al. [18] have proposed two methods by which the thermal conductivity can be specified. In the first dip (FD) method, the integral is evaluated at the first place where the HCACF goes negative. In the exponential fit (EF) method, an exponential function is fitted to the HCACF beyond a certain point (determined on a case by case basis), and this function is then used to calculate the contribution of the tail to the integral. Up to that point the integral is evaluated directly. In their investigation of β-silicon carbide, no significant differences are found between the predictions of these two methods.

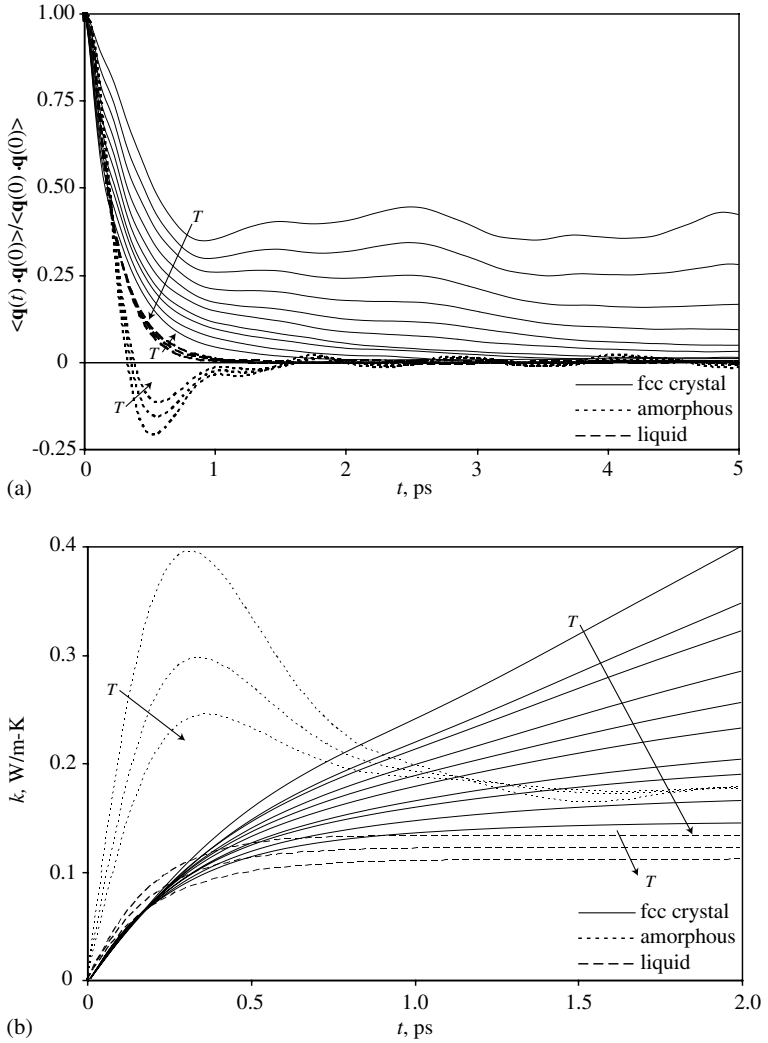

Fig. 3. Time dependence of (a) the raw HCACF and (b) its integral (the thermal conductivity) for all cases considered. Note the different time scales in the two plots. The long time behavior is shown for certain cases in Fig. 4.

The liquid HCACF shows a single stage decay, with a time scale comparable to that of the initial drop in the fcc crystal HCACF. Both the FD and EF methods are suitable for specifying the thermal conductivity. The amorphous phase HCACF shows a very different behavior. It drops below zero in the initial decay, and oscillates between positive and negative as it converges to zero. The velocity autocorrelation function for amorphous LJ argon shows a similar form [36]. We interpret this behavior as follows. In the fcc crystal, each atom experiences the same local environment. By averaging over time, the same is true for the liquid. This is not the case for the amorphous solid, where each atom has a distinct local environment. At short time scales, atoms near their equilibrium positions experience the free trajectory of a liquid atom. When the atom eventually feels the effects of the other atoms, the trajectory changes. Because the intended trajectory cannot be completed, the correlation goes negative. The time scale for this behavior is comparable to that of the liquid HCACF. The FD and EF methods are not appropriate here, and the thermal conductivity must be found from a direct specification of the integral.

In the following section, a method by which the fcc crystal HCACF (and thus the thermal conductivity) can be decomposed is presented. The results will be used to understand the form of the HCACF, and the resulting thermal conductivity trends and magnitudes.

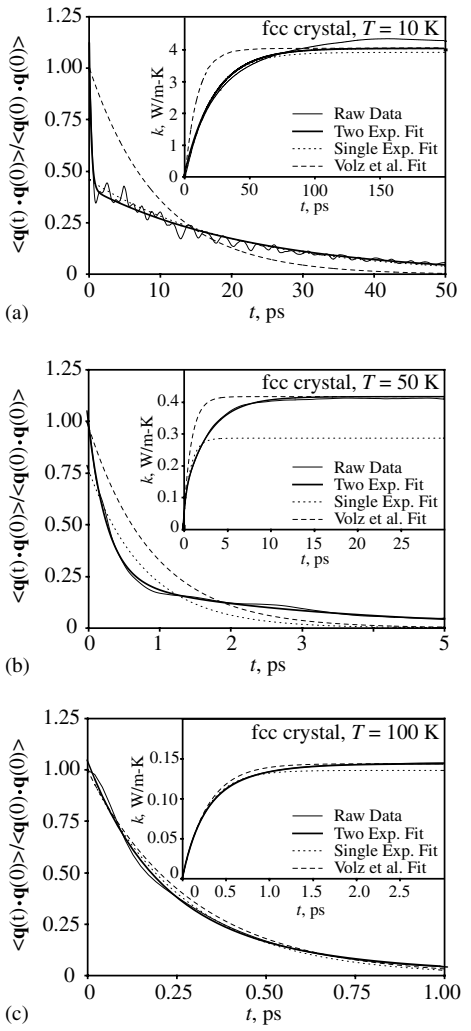

Fig. 4. The time variation of the raw HCACF and thermal conductivity, and the fits of one and two term exponential functions and the model of Volz et al. [41], for the fcc crystal at $T =$ (a) 10 K, (b) 50 K, and (c) 100 K. Note the different time scales on the HCACF and thermal conductivity plots for each condition. For a number of cases, the raw data and two term exponential fits are indistinguishable.

5.2. Thermal conductivity decomposition and results

5.2.1. Decomposition model

Based on the observed shape of the fcc crystal HCACF, it can be fitted to a sum of two exponential functions as

$$\frac{\langle \mathbf{q}(t)\cdot\mathbf{q}(0)\rangle}{3} = A_{\mathrm{ac,sh}}\exp(-t/\tau_{\mathrm{ac,sh}}) + A_{\mathrm{ac,lg}}\exp(-t/\tau_{\mathrm{ac,lg}}), \tag{15}$$

as suggested by Che et al. [21]. With Eq. (4), the thermal conductivity is then

$$k = \frac{1}{k_{\mathrm{B}}VT^2}\left(A_{\mathrm{ac,sh}}\tau_{\mathrm{ac,sh}} + A_{\mathrm{ac,lg}}\tau_{\mathrm{ac,lg}}\right) \equiv k_{\mathrm{ac,sh}} + k_{\mathrm{ac,lg}}. \tag{16}$$

In Eqs. (15) and (16) the subscripts ac, sh, and lg refer to acoustic, short range, and long range, respectively. The nature of the HCACF and thermal conductivity decompositions will be described in the following paragraph and in Sections 5.2.2 and 5.2.3. The two stage decay in the HCACF was first observed by Ladd et al. [13]. It is in contrast to the Peierls theory of thermal conductivity, which has been found to be consistent with a single stage decay of the HCACF [13,22]. Kaburaki et al. [17] suggest that the two stages in the HCACF represent contributions from local dynamics and the dynamics of phonon transport, each having a time constant τ and strength A. The use of the term 'local' is questionable, as in a crystal, there are no localized vibrational modes. Che et al. [21] associate the initial, fast decay of the HCACF with optical phonons, which cannot be the case here, as the unit cell is monatomic. The fit curves for the HCACF and thermal conductivity for temperatures of 10, 50, and 100 K are shown in Fig. 4(a)–(c), respectively. The fit captures the two stage decay very well at all temperatures. The fits of a single exponential function with time constant τ_1, according to

$$\frac{\langle \mathbf{q}(t)\cdot\mathbf{q}(0)\rangle}{3} = A_1\exp(-t/\tau_1), \tag{17}$$

are also shown in Fig. 4(a)–(c) for temperatures of 10, 50, and 100 K, respectively. The agreement with the raw HCACF is reasonable at low and high temperatures, but poor at the intermediate temperatures. The decomposition parameters (τ and A, where appropriate) and resulting thermal conductivities for all cases considered are given in Table 1.

We interpret the two stage behavior of the fcc crystal HCACF, and the resulting decomposition of the thermal conductivity into two distinct components, in the context of the phonon mean free path. While the mean free path is generally taken to be an averaged quantity (over all phonons in a system, as given by Eq. (2), or over those of a given phonon mode, as given by Eq. (1)), it can be applied to an individual phonon. For a given phonon mode, there will thus be some continuous distribution of mean free paths. Physically, the lower bound on the mean free path is given by half of the phonon wavelength (the CP limit). We believe that the first part of the thermal conductivity decomposition ($k_{\mathrm{ac,sh}}$) takes into account those phonons with a mean free path equal to one half of their wavelength. Phonons with a longer mean free paths are accounted for by the second term ($k_{\mathrm{ac,lg}}$), which has a longer decay time. The suitability of this model is assessed in the next two sections, and in Section 4 of Part II.

5.2.2. $k_{ac,sh}$: short range component

As shown in Table 1, with the exception of the 100 K value, $k_{ac,sh}$ shows little temperature dependence. The average value (and spread) of the results is $0.094^{+0.012}_{-0.016}$ W/m K. This type of behavior has been previously noted [22], and we believe that it is a result of the coordination of the atoms remaining constant as the density changes. This point will be further discussed in Section 4.4 of Part II.

Between temperatures of 40 and 80 K, there is an agreement to within 7% between $\tau_{ac,sh}$ and τ_{nn} (which was introduced and discussed in Section 4.2). Thus, the first time scale in the HCACF decomposition is related to how long it takes for energy to move between nearest neighbor atoms. In additional studies (not reported here), we have not observed any simulation cell size effects on the magnitude of $\tau_{ac,sh}$ or $k_{ac,sh}$ in the LJ argon system, suggesting that the associated phonons are in the higher frequency range of the acoustic branches (i.e., those with wavelengths on the order of a few atomic spacings). From a real space perspective, one can imagine the movement of a phonon through a system as a series of energy transfers between neighboring atoms. For a phonon with a mean free path on the order of its wavelength (as assumed for $k_{ac,sh}$), this will correspond to a few $\tau_{ac,sh}$, which explains why this is the time scale found in the decomposition. This component of the thermal conductivity is thus strongly a function of the coordination of the atoms.

To understand the difference between $\tau_{ac,sh}$ and τ_{nn} at the low temperatures, consider Fig. 2. As the energy correlation curves have been normalized, the increasing height of the first peak with increasing temperature can be interpreted as an indication of the increasing importance of $k_{ac,sh}$ to the total thermal conductivity. When the temperature is 10 K, $k_{ac,sh}$ only contributes 2% to the thermal conductivity and the peak is not evident (although there is a shoulder in the curve near the other first peaks). At temperatures of 20 and 30 K, the dominance of the long range acoustic modes leads to an underestimation of τ_{nn} from the energy correlation data. To understand the difference between $\tau_{ac,sh}$ and τ_{nn} at the high temperatures, we note that when $\tau_{ac,lg}$ approaches $\tau_{ac,sh}$ (which happens as the temperature is increased), the HCACF fitting procedure is not as accurate. Based on the consistency of the τ_{nn} results at the high temperatures, we believe that the difference between the values of $\tau_{ac,sh}$ and τ_{nn} is a numerical effect.

5.2.3. $k_{ac,lg}$: long range component

The idea of the crystalline thermal conductivity being made up of temperature dependent and independent components has been explored previously in attempts to interpret experimental data [38,39]. In the decomposition given by Eq. (16), all of the temperature dependence of the thermal conductivity is contained in $k_{ac,lg}$. This component can be investigated using the energy correlation function approach. Self-energy correlations (i.e., an autocorrelation), similar to the nearest neighbor correlations shown in Fig. 2, are plotted in Fig. 5 for temperatures of 10, 20, 50, and 100 K. While there is coherent behavior over long time periods at the low temperatures, this effect diminishes as the temperature increases (this is also seen in the long time behavior for

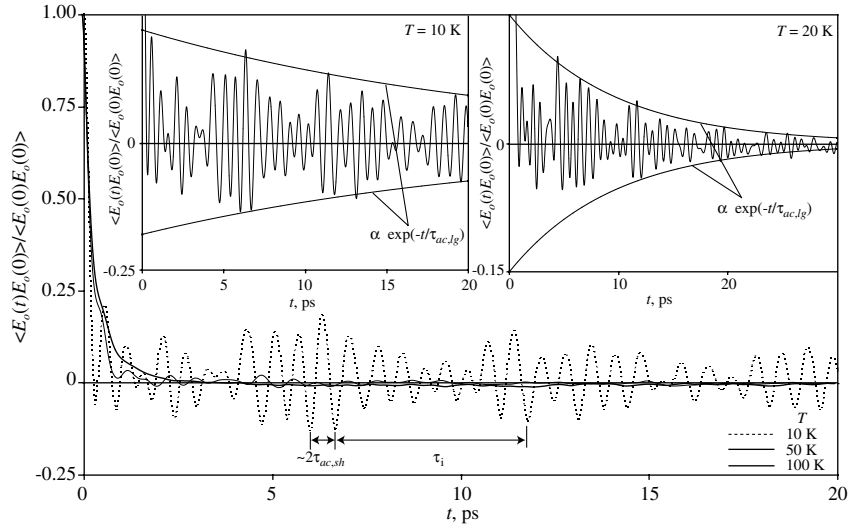

Fig. 5. Particle energy autocorrelation functions for the fcc crystal at $T = 10$, 50, and 100 K. The energy data correspond to deviations from the mean values. Note the diminishing long time coherence as the temperature is increased. The inset plots show a smaller scale for the vertical axis for the $T = 10$ and 20 K cases, along with curves representing the decay time associated with $k_{ac,lg}$.

the nearest neighbor energy correlation functions, shown in the inset of Fig. 2). This is consistent with the temperature trends in $\tau_{ac,lg}$ and $k_{ac,lg}$. For temperatures of 10 and 20 K (shown separately in the insets of Fig. 5), exponentials with time constants equal to the appropriate $\tau_{ac,lg}$ from the thermal conductivity decomposition are superimposed. The trends in the energy correlation curves are well bounded by the exponentials. The manifestation of both $\tau_{ac,sh}$ (described in Section 5.2.2) and $\tau_{ac,lg}$ outside of the HCACF supports the use of energy correlation functions for understanding heat transfer in the real space coordinates. We believe that the intermediate time scale in the long time behavior at lower temperatures (shown as τ_i in Fig. 5 for the 10 K curve) is associated with the periodic boundary conditions.

It is interesting to note that the long time scale behavior is made up of successive short time scale interactions ($\tau_{ac,sh}$, also shown in Fig. 5). At the lower temperatures, the atom to atom interactions propagate step by step, leading to behavior with a period of $2\tau_{ac,sh}$ over the long time scale. At higher temperatures, as the phonon mean free path gets smaller, the overall behavior approaches that of a damped oscillator (i.e., a monotonic decay), as opposed to a set of coupled oscillators (as seen at low temperatures), which can gain and lose energy.

5.2.4. Comparison of thermal conductivity decomposition to other integral specification techniques and to experimental data

For a series of five sets of five simulations at a temperature of 50 K for the fcc crystal (data not given), the thermal conductivities calculated with Eq. (16) fall within a range of 4.1% of their average value. We expect this error to increase as the temperature decreases, and longer correlation times are required for convergence. The time constants $\tau_{ac,sh}$ and $\tau_{ac,lg}$ fall within ranges of 1.4% and 7.1% of their average values, respectively. We expect the error in the time constants to increase as the temperature increases. As $\tau_{ac,sh}$ and $\tau_{ac,lg}$ approach similar values, the resolution of the two modes becomes more difficult, even though the accuracy of specifying the thermal conductivity increases.

The thermal conductivity predicted by the fit of a single exponential function (Eq. (17), data not given) to the fcc crystal HCACF agrees with the prediction of the fit of the sum of two exponentials (Eq. (15), data given in Table 1) to within 2.9% and 5.8% at the temperature extremes of 10 and 100 K, respectively (see Fig. 4(a) and (c)). At the intermediate temperatures, the difference between the two predictions is as much as 31% (at a temperature of 50 K, see Fig. 4(b)). This confirms the importance of considering the two stage decay. The success of the single exponential function at low temperatures is due to the dominance of $k_{ac,lg}$. At high temperatures, the single exponential succeeds because the two time constants have similar values.

For the fcc crystal, the direct specification of the integral and the FD method (data not given) agree to within 2% at all temperatures. The thermal conductivities calculated by the fit of Eq. (15) to the HCACF between temperatures of 30 and 100 K (data given in Table 1) agree with the direct specification and FD predictions to within 4%. At temperatures of 10 and 20 K, the fit gives values 7.5% and 6.5% lower than the FD method. At these low temperatures, the exponential decay is not able to fully capture the long tail. A similar finding, although more severe, has been made by Schelling et al. for silicon at a temperature of 1000 K [29]. They find that a single exponential fit to the HCACF gives a thermal conductivity value 42% lower than that found from the direct specification of the integral. The thermal conductivities studied are around 50 W/m K, so that based on our prediction of the order of $k_{ac,sh}$, considering two exponentials would not affect the results. They indicate that such exponential fits are not suitable. We do not find evidence to support this in the current simulations, which may be due to the lower thermal conductivity values involved. The fit value is used in subsequent calculations.

The fit of a single exponential to the liquid HCACF predicts a thermal conductivity (given in Table 1) that agrees with that predicted by the direct specification and FD methods (data not given) to within 3% for all cases, justifying the assumed functional form. The amorphous phase HCACF cannot be fit to a specific functional form. Its thermal conductivity is specified directly from the integral. The amorphous results are independent of temperature. We attribute this to the small temperature range studied, the approximately constant specific heat in the classical MD simulations, and the attainment of the CP limit (i.e., the mean free path is a minimum, and equal to one half of the wavelength of a given mode). Further discussion of the amorphous phase thermal conductivity is given in Part II with respect to amorphous silica.

The predicted thermal conductivities, experimental values [40], and the CP limit for argon are shown in Fig. 6 as a function of temperature. The fcc crystal MD results are in reasonable agreement with the trend and magnitude of the experimental data (a decrease above the experimental peak value, which is near a temperature of 6 K), justifying the neglection of quantum effects. The data are in better agreement than those of Li [22] when compared to the experimental data, which can be attributed to the larger cutoff used here in the MD simulations. The experimental liquid data correspond to saturation conditions, and agree very well with the MD predictions.

As given in Eq. (3), the CP limit is a quantum, harmonic expression. The MD simulations are classical and

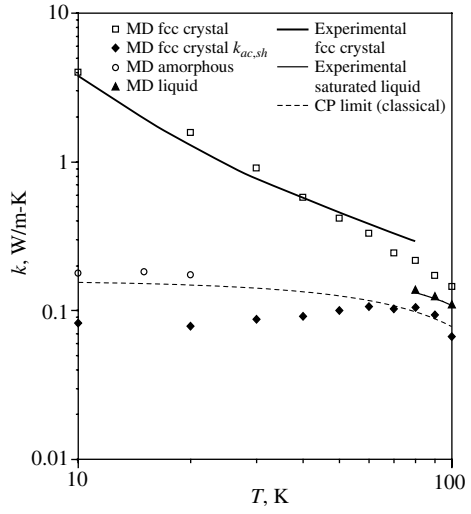

Fig. 6. Temperature dependence of the experimental and predicted LJ argon thermal conductivities.

anharmonic. As such, for use in Fig. 6, we take the classical limit of Eq. (3) (i.e., the mode specific heat $k_B x^2 e^x/(e^x-1)^2$ equal to k_B), to give

$$k_{CP} = \frac{1}{2}\left(\frac{\pi}{6}\right)^{1/3} \beta k_B n^{2/3} \sum_i u_i. \tag{18}$$

The number density is taken from the fcc crystal MD results. Due to anharmonic effects at finite temperatures, the specific heat will deviate from the classical-harmonic value, which is accounted for by the factor β. The specific heat can be calculated from the MD simulations as the rate of change of the total system energy as a function of temperature at constant volume. The results for the fcc crystal are well described by a linear fit to the data, given by

$$\beta = 0.996 - 0.000905(1/\mathrm{K})T, \tag{19}$$

where the temperature is in Kelvin. The amorphous specific heat results fall within one percent of the fcc crystal data. As the temperature increases, anharmonic effects become more important, and the deviation from the classical-harmonic value of the specific heat increases. Eq. (19) is used over the entire temperature range in the evaluation of Eq. (18). The temperature dependence of the sound speeds is obtained from quasi-harmonic dispersion curves in the [1 0 0] direction (not shown) based on the fcc crystal simulation cell sizes. There will be a difference between the amorphous sound speeds and those for the fcc crystal. As no sound speed data are available for the amorphous LJ phase, we use the fcc crystal values, scaled by a factor of 0.8 (typical for silicon and germanium [1,10]). Under these approximations, the CP limit is plotted with the understanding that there will be some error in the calculated values.

Based on the association of $k_{ac,sh}$ with k_{CP} we might expect that $k_{ac,sh}$, $k_{amorphous}$, and k_{CP} would be the same. However, as shown in Fig. 6, this is not the case. There are a number of possible explanations. First, as discussed in the previous paragraph, the calculated k_{CP} contains a number of approximations, so that the observed differences (a factor of about two) may be acceptable. Secondly, the mean free paths in the amorphous phase may actually be larger than half of the associated wavelength, leading to a larger value than $k_{ac,sh}$. We note that in additional studies (not shown), we have not found any size dependence of $k_{amorphous}$, so that the artificial periodicity imposed by the use of periodic boundary conditions is not a factor. In the liquid phase, the thermal conductivity drops below the fcc crystal value to near $k_{ac,sh}$. Once the solid phase has been eliminated, only short range interactions are important. The lack of fixed atomic positions in the liquid leads to an improved efficiency of these interactions in the transfer of heat, a shorter time constant, and a slightly higher thermal conductivity than $k_{ac,sh}$.

5.3. Time constant comparison

For the fcc crystal, the time constants $\tau_{ac,sh}$, $\tau_{ac,lg}$ and τ_1 have been obtained in Section 5.2.1 by fitting exponential functions to the HCACF. In this section, two additional time constants are obtained.

From the transient heat conduction energy equation, the time scale associated with the diffusion of heat (the transient diffusion time, τ_{td}) can be estimated as [41]

$$\tau_{td} = \frac{l_{td}^2}{(2\pi)^2 \alpha}. \tag{20}$$

Here, the length scale l_{td} is taken as $\tau_{ac,lg} u$, where u is an averaged phonon speed of sound, determined from the [1 0 0] direction quasi-harmonic dispersion curves as

$$\frac{3}{u^2} = \sum_i \frac{1}{u_i^2}. \tag{21}$$

The summation in Eq. (21) is over the three sound modes of the crystal. In Eq. (20), α is the thermal diffusivity, approximated here as $k/\rho c_v$. The specific heat is calculated directly from the MD simulations as discussed in Section 5.2.4.

For time scales shorter than τ_{td}, the results of Volz et al. [41] (who refer to it as the hydrodynamic time) indicate that the HCACF should be of the form

$$\frac{\langle \mathbf{q}(t)\cdot\mathbf{q}(0)\rangle}{3} = \frac{\langle \mathbf{q}(0)\cdot\mathbf{q}(0)\rangle}{3}\exp(-t/\tau_V), \tag{22}$$

so that from Eq. (4),

$$\tau_V = \frac{3kT^2 V k_B}{\langle \mathbf{q}(0)\cdot\mathbf{q}(0)\rangle}. \tag{23}$$

We specify a criterion of $\tau_{ac,lg}$ less than τ_{td} for the use of this formulation, allowing our data to be used at temperatures of 80 K and below. It is interesting to note that Volz et al. associate τ_V with the time constant in the hyperbolic heat conduction equation. At time scales on the order of τ_V, this equation predicts an exponential decay of the HCACF, consistent with the observed form from MD.

The time constants $\tau_{ac,sh}$, $\tau_{ac,lg}$, τ_1 and τ_V are all decay times associated with the HCACF in the GK method. The mode dependent kinetic theory time constants, $\tau_{K,i}$, given by Eq. (1), are different. They are associated with the behavior of a specific phonon mode i. To make a comparison with $\tau_{ac,sh}$, $\tau_{ac,lg}$, τ_1, and τ_V, the integrated kinetic theory time constant, τ_K, must be considered. To obtain τ_K, the MD results for the thermal conductivity are used. The speed of sound and specific heat are calculated in the same manner as described for τ_{td}.

The time constants τ_1, τ_K, and τ_V are given in Table 2. In Fig. 4(a)–(c), the raw HCACF, and the fits of Eqs. (15), (17), and (22) are shown for temperatures of 10, 50, and 100 K, respectively. For the sake of completeness, we include the τ_V data and fits at all temperatures. The fits of one and two term exponentials have been discussed in Section 5.2. The Volz et al. model, which forces the thermal conductivity and zero time intercept of the HCACF to match the raw data, only gives a reasonable fit at high temperatures, when $\tau_{ac,lg}$ is on the order of $\tau_{ac,sh}$.

The single mode time constants τ_1 and τ_V fall in between those from the thermal conductivity decomposition, $\tau_{ac,sh}$ and $\tau_{ac,lg}$. The value of τ_1 shows a transition between $\tau_{ac,sh}$ and $\tau_{ac,lg}$ as the contribution of $k_{ac,lg}$ to the thermal conductivity decreases. Volz et al., who only consider high temperatures and pressures (giving thermal conductivities greater than 4 W/m K), find agreement between τ_K and τ_V to within 7%. They attribute the good agreement to both models having been derived from the BTE. They argue that the agreement is dependent on the existence of a single stage relaxation. Based on the high thermal conductivities they find, and on our specification of $k_{ac,sh}$ near 0.1 W/m K, this may be a valid assumption for the cases considered. In the current calculations, the agreement between τ_K and τ_V is poor, which is most likely due to the lower thermal conductivities considered. In fact, the value of τ_K seems to be approaching a constant value as the temperature increases, consistent with an approach to the CP limit behavior. The high temperature agreement between τ_V and τ_1 suggests that our criteria for the use of the Volz et al. model ($\tau_{ac,lg}$ less than τ_{td}) may have been too strict.

Table 2
Time constants determined from different models for the fcc crystal

T, K	τ_1, ps	τ_K, ps	τ_V, ps
10	20.7	6.48	6.88
20	7.58	2.56	2.91
30	3.66	1.49	1.83
40	1.72	0.964	1.28
50	0.793	0.710	1.03
60	0.555	0.574	0.924
70	0.424	0.429	0.773
80	0.374	0.391	0.799
90	0.316	0.318	0.770
10	0.273	0.276	0.852

Regardless of this analysis, the single time constant approach is clearly not generally correct in a crystal. This is evident from the shape of the HCACF, and from our independent observations of the time constants $\tau_{ac,sh}$ and $\tau_{ac,lg}$ in the MD simulations. There is no evidence that the single exponential time constants are manifest in the physics of the atomic motions. They are only phenomenological quantities, convenient for simple analysis, but without any general physical interpretation.

5.4. Frequency integration and comparison to Boltzmann transport equation

The BTE can be used to predict the thermal conductivity. While MD can be used to generate the necessary input, this is an involved procedure, and has been described elsewhere [42]. However, it is still possible to investigate how the value of the thermal conductivity is obtained using the BTE by constructing a simple model.

In the MD simulations, phonon scattering is only a result of normal and Umklapp processes. The Callaway model for the thermal conductivity, obtained from the BTE under the Debye and relaxation time approximations, is given by [4]

$$k = \frac{a}{T^2}\left[\frac{1}{b_1+b_2}\int_0^{T_D/T} x^2 e^x (e^x-1)^{-2}\,dx + \frac{1}{b_1+b_2}\frac{b_2}{b_1}\frac{\left(\int_0^{T_D/T} x^4 e^x (e^x-1)^{-2}\,dx\right)^2}{\int_0^{T_D/T} x^6 e^x (e^x-1)^{-2}\,dx}\right], \quad (24)$$

where a is $k_B^2/2\pi^2 u\hbar$, and b_1 and b_2 are coefficients related to the normal and Umklapp relaxation times through

$$1/\tau_i = b_i T^3 \omega^2, \quad i = 1\ (\text{Umklapp}), 2\ (\text{normal}). \quad (25)$$

These time constants are the same as the mode dependent kinetic theory time constants, $\tau_{K,i}$. When resistive processes dominate, the thermal conductivity can be approximated by the first term of Eq. (24), which, in a classical system becomes

$$k = \frac{a}{T^2}\frac{1}{b_1 + b_2}\frac{2\pi\beta\hbar}{k_B T}\int_0^{f_D/f} \mathrm{d}f, \tag{26}$$

where f is frequency (equal to $\omega/2\pi$). The cumulative frequency dependence of the thermal conductivity is thus linear in this approximate formulation.

In the MD simulations, the thermal conductivity is calculated using the GK method from the integral of the HCACF. The integral can also be performed over frequency. The Fourier transform of the HCACF is taken, and then filtered beyond a frequency f. The inverse Fourier transform of the filtered function is taken, and integrated in time according to Eq. (4). The resulting thermal conductivity is plotted at frequency f. Note that this procedure is not the same as the GK frequency space method used by Lee et al. [14], and Volz and Chen [24] to predict the thermal conductivity.

By fitting the value of $b_1 + b_2$ in Eq. (26) to the GK thermal conductivity results, Eq. (26) and the GK frequency integral described in the previous paragraph can be compared. The results for temperatures of 10, 50, and 100 K are shown in Fig. 7(a). In the BTE approach all frequencies contribute equally to the thermal conductivity, resulting in a linear approach to the total value. The MD simulations give a very different result, placing more weight on the lower frequencies, and the total conductivity is approached asymptotically. The difference between these two approaches is a result of the frequency over which the integration is performed. While the BTE integrates over the frequencies of individual phonons (as shown in the zero temperature MD dispersion curves in Fig. 7(b)), the frequencies in the GK method are related to phonon–phonon interactions (shown through the Fourier transform of the HCACF in Fig. 7(c)). The difference between these two frequencies is equivalent to that between the phonon wavelength and its mean free path.

5.5. Suitability of Green–Kubo method

We believe that the success of the GK method in small computational cells stems from the fact that while long wavelengths cannot exist, the use of periodic boundary conditions allows for long mean free paths. This interpretation explains why significant size effects are not usually encountered in GK studies, and stresses the importance of distinguishing between these two length scales (the phonon wavelength and its mean free path) when discussing phonon transport. Along these lines, the size effects encountered when using the direct method to calculate the thermal conductivity are present because phonons are not allowed to fully decay. While long wavelength modes can exist, the mean free paths of all the allowed phonon modes are not realized. The direct method may be more appropriate for amorphous materials, where the mean free path is very small, and easily captured. However, in these cases, thermal boundary resistances at the hot and cold reservoirs are still present, and size effects may still be significant.

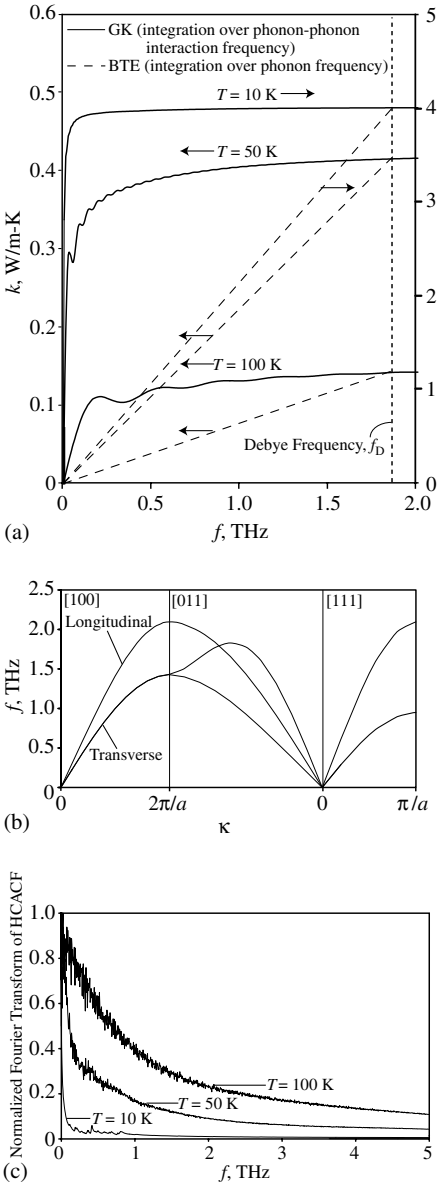

Fig. 7. (a) Comparison of the cumulative frequency dependence of the thermal conductivity from GK and BTE approaches for $T = 10$, 50, and 100 K. The 10 K curves correspond to the right vertical axis, while the 50 and 100 K curves correspond to the left vertical axis. The BTE integration is over individual phonon frequencies, while the GK frequencies correspond to phonon–phonon interaction frequencies. (b) Phonon dispersion curves calculated from the zero temperature MD configuration. a is the lattice constant and κ is the wave number. (c) Normalized Fourier transform of the HCACF for $T = 10$, 50, and 100 K.

That being said, we note that the success of the GK method in MD is not universal. For example, even with large computational cells that eliminate size effects, MD simulations of diamond at a temperature of 300 K predict a thermal conductivity of 1200 W/m K [21]. This is almost half of the experimental value of 2300 W/m K. On the other hand, MD simulations of germanium over predict the experimental room temperature thermal conductivity of 63 W/m K by a factor of two [25]. When MD results over predict the experimental thermal conductivity, it is often assumed to be because the MD system contains no impurities, which removes a source of phonon scattering. When MD under predicts the experimental results, the assumption is often that it is because the simulation cell was too small to capture long wavelength phonons. However, size effects can be taken into account, and very high purity single crystals are available in experimental investigations. As such, it is most likely that the discrepancies found between experimental data and MD-GK predictions are a result of the interatomic potentials used.

6. Summary

Using MD simulations and the GK method, the thermal conductivity of the fcc LJ argon crystal has been decomposed into two components (given by Eq. (16)). As the unit cell is monatomic, both thermal conductivity components are associated with acoustic phonons. The first component, $k_{ac,sh}$, corresponds to short wavelength acoustic phonons with mean free paths equal to one half of their wavelength (the limiting value suggested in the CP limit). The contribution of this component to the thermal conductivity is temperature independent. The second component, $k_{ac,lg}$, corresponds to acoustic phonons with mean free paths longer than one half of their wavelength. This component is temperature dependent, and dominates the magnitude of the total thermal conductivity at all but the highest temperatures considered.

The thermal conductivity decomposition gives a decay time constant for each of the two components, which have been independently observed in the simulations (see Figs. 2 and 5, and Sections 5.2.2 and 5.2.3). The decay time of the first mode corresponds to the time needed for energy to transfer between an atom and one of it nearest neighbors. The decay time for the second mode represents the average decay of those phonons with mean free paths larger than one half of their wavelength. These two time scales contrast to the single decay times used in BTE and kinetic theory approaches, which are phenomenological and only represent physical quantities under certain conditions (see Fig. 4 and Section 5.3).

In the following paper, Part II, the tools developed in this study are extended to a family of structures built from SiO_4 tetrahedra. The large unit cells of these materials lead to the existence of optical phonons, which must be included in the thermal conductivity decomposition. The variety of structures available allows for a more detailed investigation of the effects of atomic structure on thermal transport, and the development of structural metrics associated with low thermal conductivity crystals.

Acknowledgements

This work has been supported by the U.S. Department of Energy, Office of Basic Energy Sciences under grant DE-FG02-00ER45851, and the Natural Sciences and Engineering Research Council of Canada (AJHM).

References

[1] M.G. Holland, Analysis of lattice thermal conductivity, Phys. Rev. 132 (1963) 2461–2471.
[2] J.D. Chung, M. Kaviany, Effects of phonon pore scattering and pore randomness on effective conductivity of porous silicon, Int. J. Heat Mass Transfer 43 (2000) 521–538.
[3] S. Mazumder, A. Majumdar, Monte Carlo study of phonon transport in solid thin films including dispersion and polarization, J. Heat Transfer 123 (2001) 749–759.
[4] J. Callaway, Model for lattice thermal conductivity at low temperatures, Phys. Rev. 113 (1959) 1046–1051.
[5] K.C. Sood, M.K. Roy, Longitudinal phonons and high-temperature heat conduction in germanium, J. Phys.: Condens. Matter 5 (1993) 301–312.
[6] D.P. White, The effect of ionization and displacive radiation on the thermal conductivity of alumina at low temperature, J. Nucl. Mater. 212–215 (1994) 1069–1074.
[7] J.M. Ziman, Electrons and Phonons, Oxford, Oxford, 2001, pp. 288–333.
[8] A.M. Hofmeister, Mantle values of thermal conductivity and the geotherm from phonon lifetimes, Science 283 (1999) 1699–1706.
[9] D.G. Cahill, R.O. Pohl, Heat flow and lattice vibrations in glasses, Solid State Commun. 70 (1989) 927–930.
[10] D.G. Cahill, S.K. Watson, R.O. Pohl, Lower limit to thermal conductivity of disordered crystals, Phys. Rev. B 46 (1992) 6131–6140.
[11] A. Einstein, Elementare betrachtungen uber die thermische molekularbewegung in festen korpern, Ann. Phys. 35 (1911) 679–694.
[12] G.A. Slack, The thermal conductivity of nonmetallic crystals, in: F. Seitz, D. Turnbull (Eds.), Solid State Phys., vol. 34, Academic Press, New York, 1979, pp. 1–71.
[13] A.J.C. Ladd, B. Moran, W.G. Hoover, Lattice thermal conductivity: A comparison of molecular dynamics and anharmonic lattice dynamics, Phys. Rev. B 34 (1986) 5058–5064.
[14] Y.H. Lee, R. Biswas, C.M. Soukoulis, C.Z. Wang, C.T. Chan, K.M. Ho, Molecular-dynamics simulation of thermal conductivity in amorphous silicon, Phys. Rev. B 43 (1991) 6573–6580.

[15] R. Vogelsang, C. Hoheisel, G. Ciccotti, Thermal conductivity of the Lennard-Jones liquid by molecular dynamics calculations, J. Chem. Phys. 86 (1987) 6371–6375.
[16] F. Muller-Plathe, A simple nonequilibrium molecular dynamics method for calculating the thermal conductivity, J. Chem. Phys. 106 (1997) 6082–6085.
[17] H. Kaburaki, J. Li, S. Yip, Thermal conductivity of solid argon by classical molecular dynamics, Mater. Res. Soc. Symp. Proc. 538 (1998) 503–508.
[18] J. Li, L. Porter, S. Yip, Atomistic modeling of finite-temperature properties of crystalline β-SiC. II. Thermal conductivity and effects of point defects, J. Nucl. Mater. 255 (1998) 139–152.
[19] P. Jund, R. Jullien, Molecular-dynamics calculation of the thermal conductivity of vitreous silica, Phys. Rev. B 59 (1999) 13707–13711.
[20] R. Bedrov, G.D. Smith, Thermal conductivity of molecular fluids from molecular dynamics simulations: Application of a new imposed-flux method, J. Chem. Phys. 113 (2000) 8080–8084.
[21] J. Che, T. Cagin, W. Deng, W.A. Goddard III, Thermal conductivity of diamond and related materials from molecular dynamics simulations, J. Chem. Phys. 113 (2000) 6888–6900.
[22] J. Li, Modeling Microstructural Effects on Deformation Resistance and Thermal Conductivity, PhD thesis, Massachusetts Institute of Technology, Cambridge, MA, 2000.
[23] J.R. Lukes, D.Y. Li, X.-G. Liang, C.-L. Tien, Molecular dynamics study of solid thin-film thermal conductivity, J. Heat Transfer 122 (2000) 536–543.
[24] S.G. Volz, G. Chen, Molecular-dynamics simulation of thermal conductivity of silicon crystals, Phys. Rev. B 61 (2000) 2651–2656.
[25] J. Dong, O.F. Sankey, C.W. Myles, Theoretical study of lattice thermal conductivity in Ge framework semiconductors, Phys. Rev. Lett. 86 (2001) 2361–2364.
[26] P.K. Schelling, S.R. Phillpot, Mechanism of thermal transport in zirconia and yttria-stabilized zirconia by molecular-dynamics simulation, J. Am. Ceram. Soc. 84 (2001) 2997–3007.
[27] A.R. Abramson, C.-L. Tien, A. Majumdar, Interface and strain effects on the thermal conductivity of heterostructures: A molecular dynamics study, J. Heat Transfer 124 (2002) 963–970.
[28] P. Keblinski, S.R. Phillpot, S.U.S. Choi, J.A. Eastman, Mechanisms of heat flow in suspensions of nano-sized particles (nanofluids), Int. J. Heat Mass Transfer 45 (2002) 855–863.
[29] P.K. Schelling, S.R. Phillpot, P. Keblinski, Comparison of atomic-level simulation methods for computing thermal conductivity, Phys. Rev. B 65 (2002) 144306.
[30] A.J.H. McGaughey, M. Kaviany, Thermal conductivity decomposition and analysis using molecular dynamics simulations, Part II, Complex silica structures, following paper.
[31] D.A. McQuarrie, Statistical Mechanics, University Science Books, Sausalito, 2000, pp. 520–521.
[32] N.W. Ashcroft, N.D. Mermin, Solid State Physics, Saunders College Publishing, Fort Worth, 1976, pp. 395–414.
[33] D. Frenkel, B. Smit, Understanding Molecular Simulation: From Algorithms to Applications, Academic Press, San Diego, 1996, pp. 61–73.
[34] Ibid., pp. 28–37.
[35] Ibid., pp. 133–141.
[36] V.A. Luchnikov, N.N. Medvedev, Y.I. Naberukhin, V.N. Novikov, Inhomogeneity of the spatial distribution of vibrational modes in a computer model of amorphous argon, Phys. Rev. B 51 (1995) 15569–15572.
[37] Ashcroft, op. cit., p. 460.
[38] B. Wolfing, C. Kloc, J. Teubner, E. Bucher, High performance thermoelectric Tl_9BiTe_6 with extremely low thermal conductivity, Phys. Rev. Lett. 86 (2001) 4350–4353.
[39] V.A. Konstantinov, Manifestation of the lower limit to thermal conductivity in the solidified inert gases, J. Low Temp. Phys. 122 (2001) 459–465.
[40] Y. Touloukian, Thermophysical Properties of Matter, vol. 3, Plenum, New York, 1970, pp. 1–2.
[41] S. Volz, J.-B. Saulnier, M. Lallemand, B. Perrin, P. Depondt, M. Mareschal, Transient Fourier-law deviation by molecular dynamics in solid argon, Phys. Rev. B 54 (1996) 340–347.
[42] A.J.H. McGaughey, M. Kaviany, Quantitative validation of the single mode relaxation time phonon thermal conductivity model, Phys. Rev. B, submitted for publication.